Journal of Molecular Structure 984 (2010) 51–57

Contents lists available at ScienceDirect

Journal of Molecular Structure

journal homepage: www.elsevier.com/locate/molstruc

Spectroscopic, thermal and X-ray structural study of the antiparasitic and antiviral drug nitazoxanide

Flavia P. Bruno [a], Mino R. Caira [b], Gustavo A. Monti [c], Diego E. Kassuha [a], Norma R. Sperandeo [a,*]

[a] Departamento de Farmacia, Facultad de Ciencias Químicas, Universidad Nacional de Córdoba, Haya de la Torre y Medina Allende, Ciudad Universitaria, X5000HUA Córdoba, Argentina
[b] Department of Chemistry, University of Cape Town, Rondebosch 7701, South Africa
[c] Instituto de Física Enrique Gaviola, CONICET, Facultad de Astronomía, Matemática y Física, Universidad Nacional de Córdoba, Córdoba, Argentina

ARTICLE INFO

Article history:
Received 23 June 2010
Received in revised form 7 September 2010
Accepted 8 September 2010
Available online 18 September 2010

Keywords:
Nitazoxanide
Crystal structure
Solid and solution NMR
DRIFT and FTIR
Thermal analysis

ABSTRACT

Nitazoxanide [2-(acetyloxy)-*N*-(5-nitro-2-thiazolyl)benzamide, **NTZ**] is a potent antiparasitic and antiviral agent recently approved. The anti-protozoal activity of **NTZ** is believed to be due to interference with the pyruvate:ferredoxin oxidoreductase (PFOR) enzyme dependent electron transfer reaction. As drug–enzyme interactions are governed by the three-dimensional stereochemistry of both participants, the crystal structure of **NTZ** was determined for the first time to identify the conformational preferences that may be related to biological activity. **NTZ** crystallizes as the carboxamide tautomer in the orthorhombic system, space group $Pna2_1$ with the following parameters at 100(2) K: $a = 14.302(2)$ Å, $b = 5.2800(8)$ Å, $c = 33.183(5)$ Å, $V = 2505.8(6)$ Å^3, $Z = 8$, $D_x = 1.629$ g cm^{-3}, $R = 0.0319$, $wR_2 = 0.0799$ for 5121 reflections. In addition, the spectroscopic and thermal properties were determined and related to the molecular structure. The ^{13}C CPMAS NMR spectra showed resolved signals for each carbon of **NTZ**, some signals being broad due to residual dipolar interaction with quadrupolar ^{14}N nuclei. In particular, the resonance at about 127 ppm showed multiplicity, indicating more than one molecule in the asymmetric unit and this is consistent with the crystallographic data. The DSC and TG data revealed that **NTZ** shows a single DSC melting peak with extrapolated onset at 201 °C which is accompanied by a TG weight loss, indicating that **NTZ** melts with decomposition.

1. Introduction

Intestinal parasitic infections rank among the most significant causes of morbidity and mortality in the world today. Nevertheless, it has been ≥30 years since the introduction of any new innovative treatment and, for some pathogens there is currently no accepted specific therapy [1].

Nitazoxanide [2-(acetyloxy)-*N*-(5-nitro-2-thiazolyl)benzamide, **NTZ**] (Fig. 1) is a nitrothiazole derivative notable for its activity in treating both intestinal protozoal and helminthic infections. It was patented in 1976 [2,3], and since 1996, **NTZ** has been marketed in most of Latin America and has been studied worldwide. The US Food and Drug Administration (FDA) approved oral suspension of **NTZ** in December of 2002 for the treatment of diarrhea caused by *Cryptosporidium* species and *Giardia intestinalis* in pediatric patients 1–11 years of age, and in July 2004, **NTZ** was approved for treatment of diarrhea caused by *G. intestinalis* in adults. It is the first and only US FDA-approved drug for treatment of *Cryptosporidium* infection and is the first new drug approved for treatment of *Giardia* infection in ≥40 years [1]. **NTZ** is also active against numerous other parasitic and microbial pathogens, including *Trypanosoma cruzi*, the causative agent of American trypanosomiasis (Chagas disease) and *Leishmania mexicana* [4], and the ulcer-causing pathogen *Helicobacter pylori* [5]. **NTZ** is also a potent inhibitor of *Hepatitis B* and *C* virus replication [6], being proposed for the treatment of chronic viral hepatitis [7].

The anti-protozoal activity of **NTZ** is believed to be due to interference with the pyruvate:ferredoxin oxidoreductase (PFOR) enzyme dependent electron transfer reaction which is essential to anaerobic energy metabolism [8]. Thus, as drug–enzyme interactions are governed by the three-dimensional stereochemistry of both participants, the crystal structure of **NTZ** was determined to identify the conformational preferences that may be related to biological activity. In addition, since at present **NTZ** is formulated in the solid state as the active pharmaceutical ingredient (API) of both suspensions and tablets, and little is known about its physicochemical properties, we present here a spectroscopic and thermal study of **NTZ** by means of solid state and solution nuclear magnetic resonance spectroscopy (SSNMR and SNMR), diffuse reflectance infrared Fourier transform (DRIFT), Fourier transform infrared (FTIR), differential scanning calorimetry (DSC), thermogravimetry

* Corresponding author. Tel.: +54 351 4334163.
E-mail address: nrscor@fcq.unc.edu.ar (N.R. Sperandeo).

0022-2860/$ - see front matter © 2010 Elsevier B.V. All rights reserved.
doi:10.1016/j.molstruc.2010.09.006

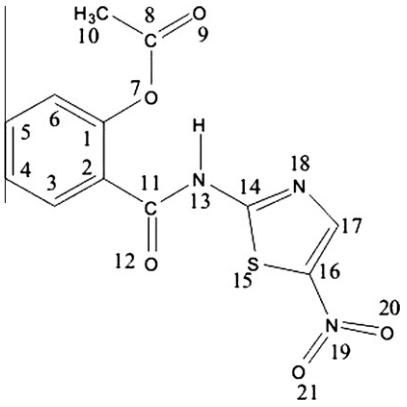

Fig. 1. Scheme of the molecule of nitazoxanide (**NTZ**) and atomic numbering used in this study.

(TG) and hot stage microscopy (HSM). The data obtained provide a meaningful set of solid state characteristics of **NTZ** that are, for the first time, reported and correlated to its crystal structure.

2. Experimental

2.1. Materials

Nitazoxanide commercial raw powder (**NTZ-r**) was purified by recrystallization from ethyl acetate (**NTZ-EA**). The purity of the isolated crystals was checked by thin layer chromatography (TLC) and DSC. For TLC analysis, pre-coated plates of silica gel 60 F254 (Merck) were used. Spots were visualized with UV light and iodide vapors. Single crystals were grown from a hot saturated filtered solution of **NTZ** in ethyl acetate. By slow evaporation of the solvent at room temperature (RT, 25–30 °C), suitable crystals for X-ray analysis were obtained. All other chemicals and solvents were of analytical reagent grade or spectroscopic quality.

2.2. Single-crystal X-ray structure determination

A roughly equant crystal specimen was cut from a plate, mounted on a Bruker DUO Apex II diffractometer (Mo Kα-radiation, $\lambda = 0.71073$ Å) and cooled in a constant stream of nitrogen vapor at 100(2) K to optimize the diffraction quality. Program APEX2 was used for data-collection [9]. Data reduction (including face-indexing absorption corrections) and unit cell refinement were performed using SAINT-Plus [10]. Laue symmetry *mmm* indicated the orthorhombic system and systematic absences corresponded to the possible space groups *P*nma and *P*na2$_1$. Intensity statistics favoured the non-centrosymmetric space group *P*na2$_1$ and attempts to solve the structure in *P*nma failed. Direct methods (program SHELXS-97 [11]) readily yielded a structural model comprising the two crystallographically independent molecules expected in *P*na2$_1$ for $Z = 8$. This model refined satisfactorily, all non-H atoms being treated anisotropically in full-matrix least-squares refinement on F^2 (SHELXL-97 [11]). All H atoms were located in difference Fourier syntheses and were included in idealised positions in a riding model with isotropic temperature factors 1.2–1.5 times those of their parent atoms.

2.3. Differential scanning calorimetry (DSC), thermogravimetry (TG) and hot stage microscopy (HSM)

The DSC and TG measurements were recorded on MDSC 2920 and TG 2950 analyzers (TA Instruments Inc., USA), respectively, at a heating rate of 10 °C min^{-1} under N_2 (99.99% purity, flow rate of 50 mL min^{-1}). For DSC measurements, crimped aluminium pans were used. The DSC and TG temperature axes were calibrated with indium (99.99% purity, *m.p.* 156.6 °C) and the Curie point of Ni (358.1 °C), respectively. Empty aluminium pans were used as references. Samples with mass 1–2 mg were employed. Data were treated with Universal Analysis 2000 software (TA Instruments Inc.).

The physical and morphological changes of the samples that occurred during the process of heating were observed through a microscope fitted with a Kofler hot-stage (Leitz, Wetzlar, Germany) at a constant rate of about 8 °C min^{-1} from RT. In order to provide experimental conditions similar to those of the DSC studies, the samples were not immersed in silicone oil. All the observations were made at a 30× magnification.

2.4. NMR spectroscopy

High resolution ^{13}C SSNMR spectra were recorded using the ramp CPMAS sequence with proton decoupling during acquisition. The experiment was performed at RT in a Bruker Avance II 300 (Bruker, Germany) spectrometer, operating frequency for carbons 75 MHz, equipped with a 4 mm MAS probe. Spinning rate was 8 kHz. The recycling time was 20 s, the contact time during CP was 2 ms, and 2048 scans were recorded. SPINAL64 sequence was used for decoupling during acquisition with a proton field H_{1H} satisfying $\omega_{1H}/2\pi = \gamma_H H_{1H}/2\pi = 62.5$ kHz. Chemical shifts were quoted with respect to tetramethylsilane (TMS) and measured via replacement with adamantane (29.50 and 38.56 ppm). Interrupted decoupled experiments were conducted using a 40 μs delay before acquisition. Heteronuclear ^{1}H–^{13}C correlation experiments were performed in the CPMAS mode with contact time of just 100 μs; only protons directly bonded to carbon were detected. Frequency shift Lee–Gooldburg proton homonuclear decoupling was used during the evolution time at a 100,000 kHz decoupling power. The number of increments in the indirect dimension was 64 with an increment step of 43 μs.

The ^{1}H and ^{13}C NMR characteristics of **NTZ** in $CDCl_3$ and DMSO-d_6 solutions were studied at 25 °C using corresponding ^{1}H and ^{13}C NMR spectra [Bruker Avance II 400 spectrometer current probe 5 mm BBI 1H/D-BB Z-GRD Z8202/0349] along with two-dimensional COSY-45, HSQC and HMBC. The ^{1}H NMR spectra were obtained with a spectral width of 20 ppm using a 30° pulse (7.09 μs) and 16 scans. The ^{13}C NMR spectra were recorded operating at 100 MHz and were obtained using the following acquisition parameters: spectral width, 220 ppm; relaxation delay, 1.7 s; 2048 scans for sample, and a 30° excitation pulse. The COSY-45 spectrum (DMSO-d_6) was obtained using gradient pulses for selection, and the following acquisition parameters: scans, 2; relaxation delay, 1 s; f1 channel 30° high power pulse (7.09 μs) and sizes of fid of 256 (time domain 1) and 2048 (time domain 2). The HSQC spectrum (DMSO-d_6) was obtained using four scans, an 1 s relaxation delay, a f1 channel 30° high power pulse of 7.09 μs, sizes of fid equal to those of the COSY-45 spectrum, and a one-bond C–H coupling constant of 145 Hz. The HMBC spectrum (DMSO-d_6) was obtained using acquisition parameters identical to that of the HSQC spectrum but the scans were 8, and a more than one-bond C–H coupling constant of 8 Hz was used. The center of the solvent peak was used as an internal standard which was related to TMS. The processing of the data was performed with a Bruker Standard program (TOPSPIN 2.0).

2.5. Diffuse reflectance infrared Fourier transform (DRIFT) and Fourier transform infrared (FTIR) spectroscopy

FTIR and DRIFT spectra were recorded on a Nicolet Avatar 360 FTIR spectrometer (Nicolet Instruments Corp., Madison, WI). For DRIFT spectra, a diffuse reflectance accessory and macro diffuse

reflectance cups of 13-mm diameter (~400 mg) were used. For the preparation of the blend, dry KBr was ground for 2 min before mixing with the sample (2.5% w/w) in an agate mortar with only light grinding performed. The blend was then placed in the cup, and excess material was removed by placement of a microscope slide against the open cup in a rotary motion to leave a level but roughened surface, and scanned immediately. For IR spectra, a 0.5% w/w dispersion of **NTZ** in dry KBr was prepared using the procedure described for the DRIFT blend. KBr pellets were obtained with a minipress (Hidráulicos Delfabro, Argentina) at 6 tons without any extra grinding. All the spectra were acquired accumulating 64 scans at 4 cm^{-1} resolution, and were processed with the OMNIC E.S.P. 5.1 program (Nicolet Corp.). KBr scans were used as background.

2.6. X-ray powder diffraction (XRPD)

XRPD patterns were recorded at RT with a Philips ŕPert PRO PANalytical powder diffractometer (Philips, The Netherlands). The measuring conditions were: Cu Kα-radiation, 40 kV, 40 mA, step size of 0.02° (2θ), time per step 5 s, time constant of 0.03 s, angular range 3–35° 2θ. Samples, lightly ground in an agate mortar, were measured on a single crystal Si holder.

3. Results and discussion

3.1. Crystal and molecular structure

Table 1 lists crystal data and refinement parameters for **NTZ**. Selected geometrical parameters are reported in Table 2. The crystallographic asymmetric unit, comprising two independent molecules (*a* and *b*), is shown in Fig. 2a. Chemically equivalent bond lengths in the two independent molecules are in very good agreement. Bond distances and angles in the common nitrothiazolyl moiety of **NTZ** and *N*-(4-methoxybenzyl)-*N*′-(5-nitro-1,3-thiazol-2-yl)urea [12] are also in good agreement. The individual conformations of molecules *a* and *b* are stabilised by common intramolecular hydrogen bonds N13–H···O7 (N···O = 2.700(2) Å, 2.681(2) Å for *a*, *b* respectively), indicated in Fig 2a. This interaction leads to the formation of slightly puckered six-membered rings, as is evident from the non-zero torsion angles around the bonds C2–C11 as well as the significant asymmetry resulting in the two exocyclic angles at C2. The remaining torsion angles in Table 2 reflect the extents to which the acetyl and nitro residues are tilted with respect to the phenyl and thiazolyl rings respectively. When the atomic coordinates of molecule *a* are inverted, the resulting molecule overlaps very closely with molecule *b* (rms fit 0.072 Å). In each independent molecule the phenyl and thiazolyl residues are slightly inclined to one another (angles of intersection of the respective least-squares planes: 6.8(1)° (*a*), 6.3(1)° (*b*)).

Table 1
Crystallographic data for nitazoxanide (**NTZ**).

Empirical formula	$C_{12}H_9N_3O_5S$
Formula weight	307.28
Temperature (K)	100(2)
Wavelength (Å)	0.71073
Crystal system, space group	Orthorhombic, *P*na2$_1$
Unit cell dimensions	
a (Å)	14.302(2)
b (Å)	5.2800(8)
c (Å)	33.183(5)
V (Å^3)	2505.8(6)
Z, calculated density (Mg m^{-3})	8, 1.629
Absorption coefficient (mm^{-1})	0.286
F(0 0 0)	1264
Crystal size (mm^3)	0.17 × 0.29 × 0.31
θ Range for data-collection (°)	2.85–26.55
Limiting indices	$-17 \le h \le 16$ $-6 \le k \le 6$ $-41 \le l \le 41$
Reflections collected/unique	21,925/4954
Completeness to theta	99.3%
Absorption correction	Face-indexing
Max. and min. transmission	0.9152, 0.9535
Refinement method	Full-matrix least-squares on F^2
Data/restraints/parameters	4954/1/381
Goodness-of-fit on F^2	1.046
Final *R* indices [$I > 2\sigma(I)$]	R_1 = 0.0307, wR_2 = 0.0788
R indices (all data)	R_1 = 0.0319, wR_2 = 0.0799
Flack parameter	0.03(5)
Largest diff. peak and hole (e Å^{-3})	0.88 and −0.21

Table 2
Selected bond distances, bond angles, and torsion angles for **NTZ**.

Parameter	Molecule A	Molecule B
Bond lengths (Å)		
S15–C14	1.720(2)	1.729(2)
S15–C16	1.722(2)	1.719(2)
C16–C17	1.353(3)	1.354(3)
C17–N18	1.364(4)	1.365(3)
C18–C14	1.308(3)	1.306(3)
C16–N19	1.421(2)	1.423(2)
N13–C14	1.375(2)	1.375(2)
N13–C11	1.364(3)	1.363(3)
Bond angles (°)		
C14–S15–C16	86.17(9)	86.20(9)
C1–C2–C11	126.5(2)	125.6(2)
C3–C2–C11	115.6(2)	116.3(2)
Torsion angles (°)		
C1–C2–C11–N13	−15.4(3)	15.2(3)
C11–C2–C1–O7	2.3(3)	−3.8(3)
C2–C1–O7–C8	−122.9(2)	118.0(2)
C11–N13–C14–S15	8.6(3)	−9.4(3)
S15–C16–N19–C20	4.0(2)	−3.5(2)

In addition to the N13–H···O7 hydrogen bonds, weak intramolecular H-bonds C3–H···O12 occur in both molecules *a* and *b* with C···O 2.756(2) and 2.761(2) Å respectively. The two molecules in the asymmetric unit are linked by a weak hydrogen bond C5a–H···O9b (C···O = 3.155(3) Å).

A projection of the crystal structure down the short unit cell axis (*b* = 5.2800(8) Å) is shown in Fig. 2b. In addition to the interactions described above, the crystal is stabilized by short π-stacking interactions between the thiazolyl rings of molecules *a* and *b*. These interactions, with a ring centroid–centroid distance of 3.460 Å, are shown as long dashed lines and they occur close to the 0 0 2 crystal planes.

Data from the refined single crystal X-ray structure were used to compute the idealised X-ray powder pattern for this crystalline phase (at 100 K) (Fig. 3a). As can be seen, the strongest peak in the pattern, simulated with Cu Kα-radiation (λ = 1.5418 Å), occurs at 2θ = 5.33°, with *d* = 16.59 Å. Peak indexing shows that this corresponds to the reflection from the 0 0 2 planes. The very strong peak intensity is clearly due to the fact that these planes correspond to layers that accommodate all of the 'heavy' (sulfur) atoms (Fig. 2b).

In comparing the computed pattern (Fig. 3a) with the experimental ones of **NTZ-r** and **NTZ-EA** (Fig. 3b and c), it is evident that they all represent the same phase. However, the better overall intensity match between the computed pattern and that of the commercial sample indicates a relatively low level of preferred orientation in the latter case. Instead, the sample crystallized from ethyl acetate displays a significant level of preferred orientation.

3.2. DSC, TG, NMR, DRIFT and FTIR

The DSC and TG–DTG curves (Supplementary material) of **NTZ-r** and **NTZ-EA** matched well, indicating that the samples are similar

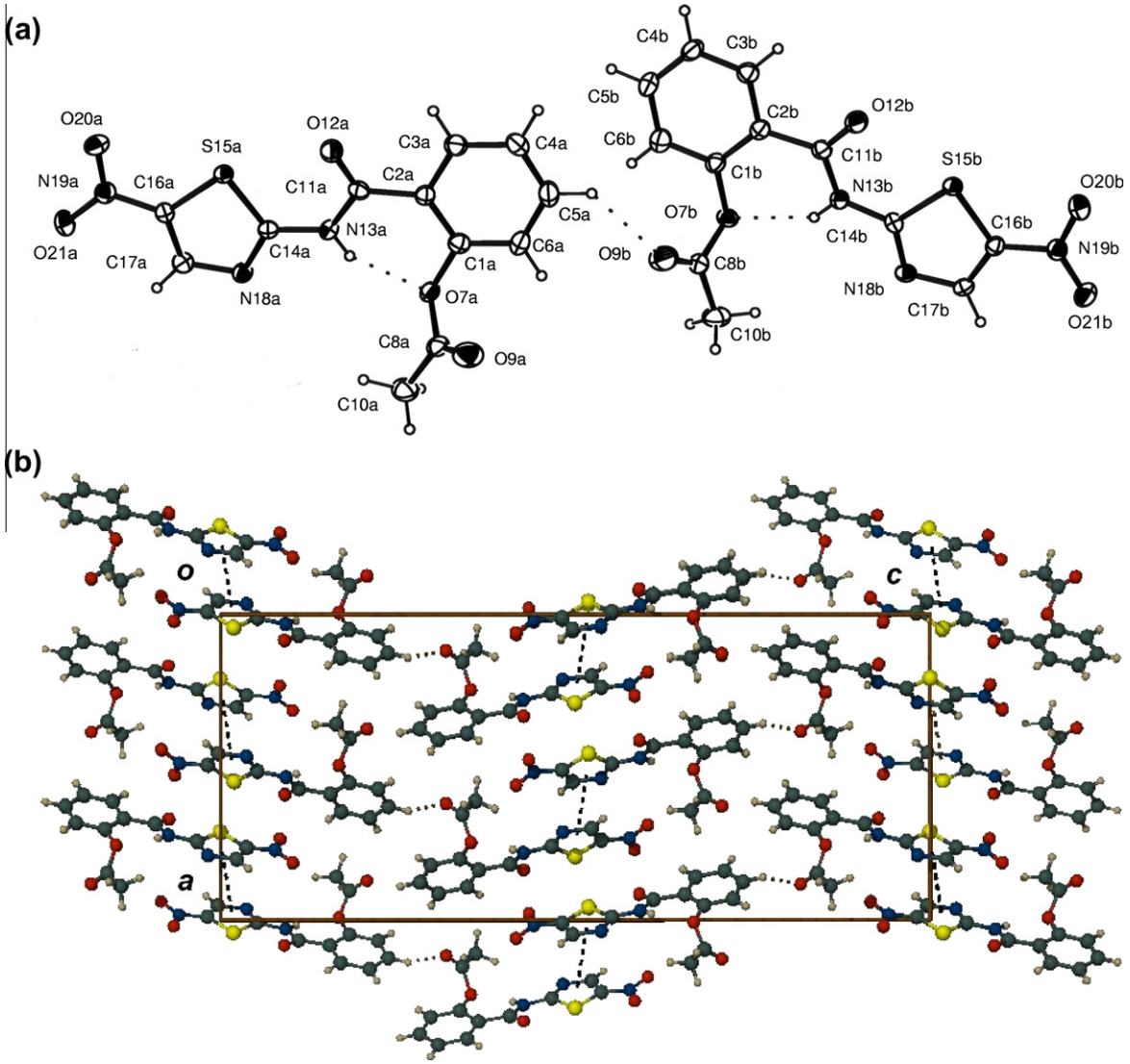

Fig. 2. ORTEP view of the asymmetric unit of **NTZ** showing the intramolecular hydrogen bond, atom labeling and non-H atoms drawn as ellipsoids at the 50% probability level (a) and molecular packing in the crystals of **NTZ** showing the intermolecular C–H···O hydrogen bonds, and π-stacking interactions (b).

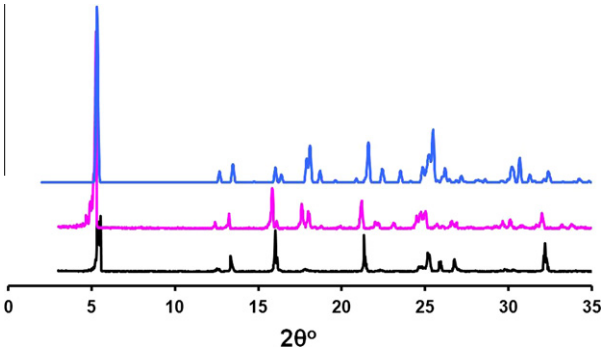

Fig. 3. Computed XRPD trace of **NTZ** calculated at 100 K (a), and experimental traces for the commercial raw powder (**NTZ-r**) (b) and the crystals obtained from ethyl acetate (**NTZ-EA**) (c).

thermically. In addition, the thermal data provided supplementary evidence that **NTZ** crystallized as a solvent-free solid. Indeed, neither DSC desolvation nor TG mass losses were observed for **NTZ-r** and **NTZ-EA** below 190.0 °C. The DSC curves (Supplementary material) exhibited only one narrow endothermic peak with extrapolated onset temperature of 201.1 °C (**NTZ-r**, ΔH = 148.6 J g^{-1}) and 201.2 °C (**NTZ-EA**, ΔH = 153.8 J g^{-1}) due to melting, which is followed by an exothermic peak ascribable to decomposition. The respective TG curves (Supplementary material) showed only one stage of weight loss that started at about 190 °C, indicating that both samples sublimed and underwent degradation under melting. The thermal events just described were supported by the observations made of **NTZ-r** and **NTZ-EA** crystals, alone or placed side by side on the same slide, using a Kofler apparatus. Microscopic observations indicated that **NTZ-r** consisted of small transparent irregular crystals while **NTZ-EA** exhibits pale yellow transparent prisms (Supplementary material). By heating **NTZ-r** and **NTZ-EA** crystals from RT to 180 °C, phase modifications or evaporation losses were not produced which is consistent with the DSC and TG–DTG results. At about 183 °C, a few small transparent prisms of **NTZ** (TLC identification of the crystals eluted with the minimum volume of ethyl acetate, using tetrahydrofuran–ethyl acetate 2:1 as mobile phase) were formed on the cover slip, indicating a partial sublimation process, and this is consistent with the TG–DTG data which indicated that the weight loss started before the fusion of the samples. On further heating, the material on the slide as well as the crystals on the cover melted; however, the

fusion range was slightly broader for **NTZ-EA** (202–6 °C) than for **NTZ-r** (201–3 °C) which may be attributed to the differences in the size and shape of the particles (Supplementary material). On further heating the molten phases darkened, typical of a decomposition process.

The ^{13}C SSNMR spectra of **NTZ-r** and **NTZ-EA** are shown in Fig. 4, while the carbon assignments and chemical shift values are given in Table 3. As Fig. 4 shows, the spectra are very similar, exhibiting well-resolved signals for each C of the molecule, though some signals are broad. In particular, the broadening of the peaks for the 11-carbonyl carbon (163.0 ppm) and C-14 (160.4 ppm) can be attributed to residual dipolar interaction with quadrupolar ^{14}N atoms. Because this interaction depends on the polar angles linking the interatomic distance to the relevant electric field gradient tensor, sometimes the effect is not very noticeable [13]. A splitting of the resonance assigned to C-4 (127.0 and 127.7 ppm) was also seen (Fig. 4b and inset), indicating that there are at least two molecules in the asymmetric unit, and this is consistent with the crystallographic data. The complete signal assignments of the ^{13}C SSNMR spectra were achieved by analyzing dipolar dephasing experiments, which yields quaternary carbons and methyl groups only, two-dimensional ^{1}H–^{13}C SSNMR heteronuclear correlation and by comparison with 1D and 2D ^{1}H and ^{13}C solution NMR experiments.

The ^{13}C SSNMR spectrum of **NTZ-EA** (Fig. 4b) was compared with those recorded in $CDCl_3$ and DMSO-d_6 solutions at similar concentrations and the data are collected in Table 3. As Table 3 shows, the chemical shifts of seven of the 12 carbons of the molecule, C-1, C-4, C-5, C-6, C-8, C-10 and C-17, measured in the solid state are close to the values observed in both solutions (the differences in chemical shifts were all less than ±1.5 ppm), indicating that the chemical environment around these carbons is very similar in the solid state and in solution [14]. In particular, the C-8 carbonyl chemical shifts are similar, and this could indicate that the weak strength of the intermolecular bond between this carbonyl and the H-5′, demonstrated in the crystal structure, does not affect the C-8 chemical shift value in the solid state. Of the remaining carbons, the C-2, C-11 and C-14 carbon chemical shifts measured in the solid state are close to the values observed in $CDCl_3$ solution, but slightly different from the values observed in DMSO-d_6 (Δsolid-solution: −3.4, −2.8 and −1.9 ppm, respectively). The observed DMSO-d_6-induced shifts (Table 3) can be attributed to the usual solvents effects and to the formation of intermolecular interactions of the molecule of **NTZ** with DMSO-d_6 through the amide proton, as

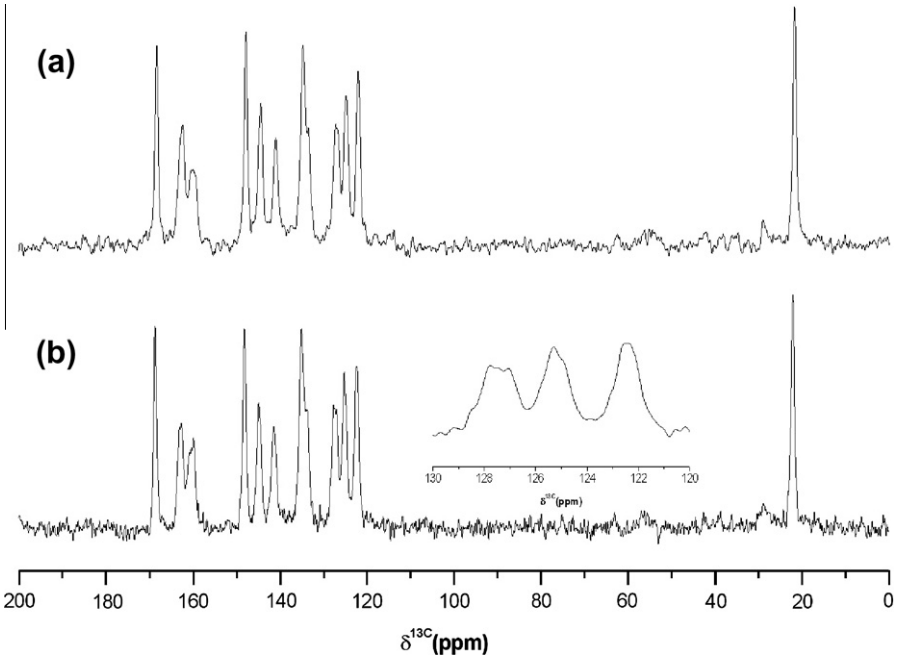

Fig. 4. ^{13}C CPMAS NMR spectra of **NTZ-r** (a) and **NTZ-EA** (b). In the inset the peaks appearing in the 130–120 ppm region are shown.

Table 3
Comparison of the ^{13}C NMR chemical shifts (in ppm) of **NTZ** in solid and solution ($CDCl_3$ and DMSO-d_6) states.

C atoms	CPMAS	$CDCl_3$ (0.062 M)	Difference (SS-$CDCl_3$)	DMSO-d_6 (0.065 M)	Difference (SS-DMSO-d_6)
1	148.3	148.7	−0.4	149.1	−0.8
2	122.5	123.6	−1.1	125.9	−3.4
3	133.9	130.7	3.2	130.3	3.6
4	127.0	126.8	0.2	126.4	0.6
4[a]	127.7	–	–	–	1.3
5	135.2	134.5	0.7	134.0	1.2
6	125.2	123.9	1.3	123.9	1.3
8	168.9	168.1	0.8	169.4	−0.5
10	22.2	21.2	1.0	21.2	1.0
11	163.0	162.9	0.1	165.8	−2.8
14	160.4	160.9	−0.5	162.3	−1.9
16	145.0	140.6	4.4	143.0	2.0
17	141.5	140.6	0.9	142.6	−1.1

[a] Independent molecule *b*.

was observed for other amides [15,16]. Of the other two carbons, C-3 showed similar chemical shifts in $CDCl_3$ and DMSO-d_6 solutions; but it is shifted to a high frequency in the solid state (Δsolid-solution: 3.2 and 3.6 ppm), and this could indicate a small change in the orientation of the amide group in the solid state [16]. With regard to C-17, very similar chemical shifts are observed for C-16 and C-17 in the ^{13}C SNMR spectra, i.e. the signals merged in $CDCl_3$, indicating a chemical equivalence of these carbons; however, two separate signals at 144.5 and 141.1 ppm with accompanying high frequency shifts of about 4 and 2 ppm, respectively, are observed for these carbons in the solid state, indicating that the chemical environments are different for these carbon atoms possibly due to further rigidities of the nitro group and thiazole ring in the solid state [14].

In light of these data, the ^1H NMR spectrum of **NTZ** was recorded in $CDCl_3$ and DMSO-d_6 solutions at similar concentrations (Table 4). As distinctive feature, the spectra display only one set of signals, like the ^{13}C SNMR spectra (Table 3), indicating that these NMR experiments did not detect different **NTZ** tautomers. This may indicate that they did not exist or if they exist the rate of tautomeric exchange was in the fast exchange limit of the NMR time scale for the solvents selected [17]. The comparison of the proton chemical shift values of the two spectra showed significant variations only for the NH proton. In fact, it was shifted in DMSO-d_6 (Table 4) to a higher frequency relative to the $CDCl_3$ solution, as much as −3.01 ppm, suggesting that a strong intermolecular interaction of **NTZ** with DMSO molecules occurs through the amide proton [15,16] and that the intramolecular N–H···O interaction seen in the solid state does not play an important role in solution in fixing the NH proton [14]. This is consistent with the DMSO-induced chemical shifts observed for various carbons of the molecule, as discussed previously.

With regard to the stability of **NTZ** in $CDCl_3$ and DMSO-d_6 solutions, though systematic stability studies have not been carried out, it was observed that it is stable at RT protected from light. In fact, the comparison of the proton spectra of the freshly prepared DMSO-d_6 and $CDCl_3$ solutions with the same ones after 15 days (DMSO-d_6) and 15 and 30 days ($CDCl_3$) (Table 4) of storage did not show any new peaks attributable to degradation products or different tautomers. The chemical shifts and the integration values (data not shown) remained unchanged, indicating that **NTZ** is stable in the assayed conditions; however, further studies are necessary to investigate the stability and tautomerism of this compound. This will be our next task.

The DRIFT spectra of **NTZ-r** and **NTZ-EA** were also compared (Fig. 5a and b). Both spectra matched well when compared, providing additional evidence that both samples are the same crystalline phase. The spectra exhibited a medium NH stretch vibration

Table 4
Comparison of the ^1H NMR chemical shifts (in ppm) of **NTZ** in $CDCl_3$ and DMSO-d_6 at different storage times (in days, d).

H atom	$CDCl_3$ (0.062 M)	$CDCl_3$ (15 d)[a]	$CDCl_3$ (30 d)[a]	DMSO-d_6 (0.065 M)	DMSO-d_6 (15 d)[a]
H-3	8.05 *dd*[b] (*J* = 7.8, 1.7 Hz)	8.05 *dd*	8.05 *dd*	7.85 *dd* (*J* = 7.8, 1.6 Hz)	7.84 *dd*
H-4	7.46 *td*[c] (*J* = 8.8, 7.9, 0.9 Hz)	7.45 *td*	7.47 *td*	7.45 *td* (*J* = 8.4, 7.6, 0.9 Hz)	7.45 *td*
H-5	7.70 *td* (*J* = 8.4, 7.9, 1.8 Hz)	7.68 *td*	7.70 *td*	7.70 *td* (*J* = 8.4, 7.8, 1.6 Hz)	7.69 *td*
H-6	7.30 *dd* (*J* = 8.3, 0.9 Hz)	7.29 *dd*	7.30 *dd*	7.32 *dd* (*J* = 8.2, 0.7 Hz)	7.34 *dd*
H-17	8.19 *s*[d]	8.21 *s*	8.23 *s*	8.70 *s*	8.70 *s*
CH_3	2.45 *s*	2.44 *s*	2.45 *s*	2.25 *s*	2.25 *s*
NH	10.61 *br s*[e]	10.51 *br s*	10.51 *br s*	13.62 *br s*	13.65 *br s*

[a] In the dark at 20–25 °C.
[b] Doublet of doublet.
[c] Triplet of doublet.
[d] Singlet.
[e] Broad singlet.

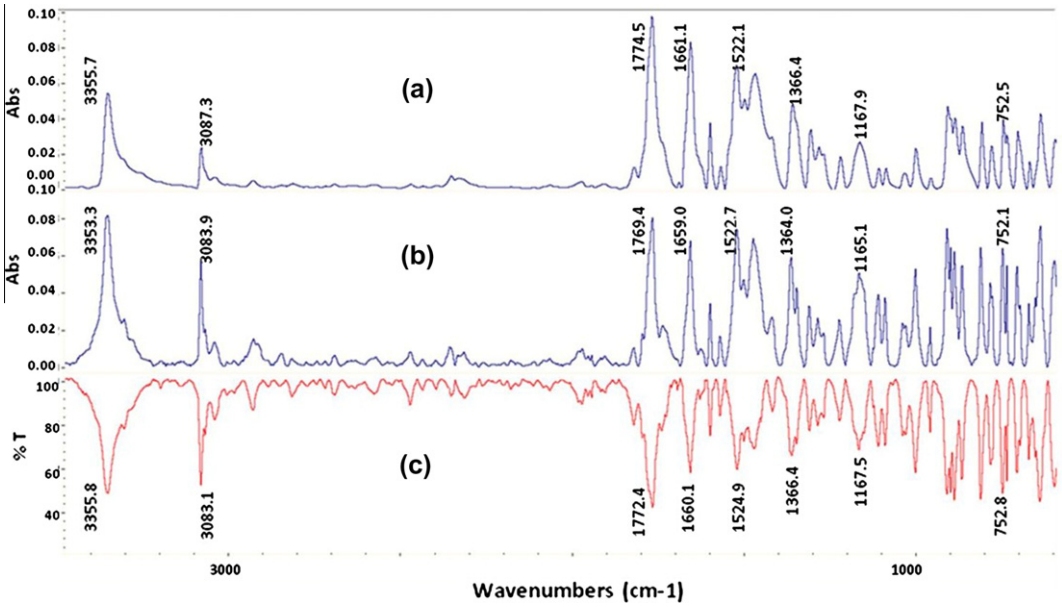

Fig. 5. DRIFT spectra of **NTZ-r** (a) and **NTZ-EA** (b), and FTIR spectrum (KBr pellet) of **NTZ-r** (c).

centered at very similar wavenumber in both samples, i.e. 3355.7 cm^{-1} (**NTZ-r**) and 3353.3 cm^{-1} (**NTZ-EA**). The intensity and the wavenumber of the band, which corresponded to the normal position for a secondary amide associated through H-bonds, is consistent with the XRD results that indicated that the NH group participates in hydrogen bonding. The spectra also showed a strong band at 1774.5/1769.4 cm^{-1} (**NTZ-r**/**NTZ-EA**) assigned to the ester carbonyl stretching mode, and a medium absorption peak at 1659.0/1661.1 cm^{-1} (**NTZ-r**/**NTZ-EA**) attributed to the amide carbonyl (C11=O) stretch. Also present in the spectra were bands at 1522.1/1522.7 cm^{-1} (**NTZ-r**/**NTZ-EA**) and 1366.4/1364.0 cm^{-1} (**NTZ-r**/**NTZ-EA**) assigned tentatively to the amide C–N stretch overlapped with the symmetrical mode of the nitro group, and to the amide N–H bend and the asymmetrical stretch of the NO_2 group, respectively.

The FTIR spectrum of **NTZ-r** (Fig. 5c) was also recorded to evaluate the effect of input of mechanical energy (6 tons). As seen in Fig. 5, the IR and DRIFT spectra of **NTZ-r** were similar enough to consider that the applied pressure did not induce any disruption of the crystal lattice.

4. Conclusions

Single crystal XRD data, solid state and solution NMR, DRIFT and thermal behavior of **NTZ** are reported here for the first time, giving a comprehensive description of the solid-state features. It was found that **NTZ** crystallized from ethyl acetate as the carboxamide tautomer. The molecular and crystal structures are stabilized by intra- (N–H···O) and intermolecular (C–H···O, π-stacking) interactions respectively, which gives a great stability to the crystal building. A reference XRPD trace for this crystal form of **NTZ** was generated from the single crystal data and was found to match the experimental trace. The chemical shift values observed for the ^{13}C SS and SNMR spectra of **NTZ** were related to the chemical environments of various carbons and protons.

Acknowledgements

Financial support from SECyT-UNC, CONICET and FONCyT of Argentina is gratefully acknowledged. F.P. Bruno and D.E. Kassuha acknowledge financial support from FONCyT and CONICET fellowships, respectively. The authors gratefully thank Dra. Carmen Pena of Roemmers of Uruguay for the generous gift of **NTZ-r**. Helpful comments on NMR solution spectra from Dra. Bonetto, who recorded the spectra, are grateful acknowledged. MRC thanks the University of Cape Town and the National Research Foundation (Pretoria) for research support.

Appendix A. Supplementary material

These include DSC and TG data, and microphotographs for **NTZ**. CCDC 775321 contains the supplementary crystallographic data for this paper. These data can be obtained free of charge at www.ccdc.cam.ac.uk/retrieving.html [or from the Cambridge Crystallographic Data Centre (CCDC), 12 Union Road, Cambridge CB2 1EZ, UK. Fax: +44 (0) 1223 336033; email: deposit@ccdc.cam.ac.uk]. Supplementary data associated with this article can be found, in the online version, at doi:10.1016/j.molstruc.2010.09.006.

References

[1] L.M. Fox, L.D. Saravolatz, Clin. Infect. Dis. 40 (2005) 1173.
[2] S. Budavari, M. O'Neil, A. Smith, P. Hechkelman, J. Obenchain, J. Gallipeau, A. Ó Arecca (Eds.), The Merck Index, 13th ed., Merck and Co., Whitehouse Station, New York, 2001. p. 1177.
[3] Y. Waknine, FDA Approvals: Revatio, Xeloda, Alinia. <http://www.medscape.com/viewarticle/507232> (accessed 20.10.09).
[4] M.J. Chan-Bacab, E. Hernández-Núñez, G. Navarrete-Vásquez, J. Antimicrob. Chemother. 63 (2009) 1292.
[5] F. Mégraud, A. Occhialini, J.F. Rossignol, Antimicrob. Agents Chemother. 42 (1998) 2836.
[6] B.E. Korba, A.B. Montero, K. Farrar, K. Gaye, S. Mukerjee, M.S. Ayers, J.F. Rossignol, Antiviral Res. 77 (2008) 56.
[7] E.B. Keeffe, J.F. Rossignol, World J. Gastroenterol. 15 (2009) 1805.
[8] J.F. Rossignol, Y.M. El-Gohari, Aliment. Pharm. Therap. 24 (2006) 1423.
[9] Bruker APEX2 Version 1.0-27, Bruker AXS Inc., Madison, Wisconsin, USA, 2005.
[10] Bruker SAINT-Plus (including XPREP), Version 7.12, Bruker AXS Inc., Madison, Wisconsin, USA, 2004.
[11] G.M. Sheldrick, Acta Crystallogr. A 64 (2008) 112.
[12] N. Vasdev, A.A. Wilson, S. Houle, A.J. Lough, Acta Crystallogr. E 63 (2007) 1653.
[13] R.K. Harris, A.C. Olivieri, Prog. NMR Spectrosc. 24 (1992) 435.
[14] M. Stoltz, D.W. Olivier, P.L. Wxasse, A.A. Chalmers, J. Pharm. Sci. 80 (1991) 357.
[15] M. Kondo, Bull. Chem. Soc. Jpn. 52 (1979) 521.
[16] C.Z. Gómez-Castro, I.I. Padilla-Martínez, F.J. Martínez-Martínez, E.V. García-Báez, Arkivoc V (2008) 227.
[17] M.T. Chenon, D.W. Grant, R.J. Pugmire, J. Org. Chem. 42 (1977) 659.